A General Framework for UAV-Aided THz Communications Subject to Generalized Geometric Loss

Osamah S. Badarneh, Faissal El Bouanani, and Fares Almehmadi

***Abstract*—In this article, we develop a general framework for the performance analysis of unmanned aerial vehicle (UAV) aided terahertz (THz) communications under generalized geometric loss, which considers the fluctuations of the UAV's position and orientation alongside the non-orthogonality of the THz beam with respect to the detector plane. In particular, we derive general and novel analytical expressions for the probability density function and the cumulative distribution function of the instantaneous signal-to-noise ratio (SNR) under generalized fading channels subject to generalized geometric loss. Consequently, novel, general, and accurate analytical expressions for the outage probability, average symbol error rate, and average channel capacity are derived. Furthermore, approximate asymptotic expressions in the high SNR regime are also derived. Moreover, A very accurate approximate expression for the channel capacity is also provided in the low SNR regime. As an example, the system performance under the α-μ fading channel model is analyzed in terms of the above-mentioned performance metrics.**

***Index Terms*—Disorientation, geometric loss, misalignment, THz communications, UAVs.**

I. Introduction

THE compound annual growth rate (CAGR) of global mobile data traffic (MDT) over the last five years has indeed been 46%, resulting in overall MDT of 77 and 1589.7 Exabytes (EB, i.e. 1.59×10^9 Terabyte (TB)) per month in 2022 and 2030, respectively [1]. In particular, the Asia Pacific region accounts for 56% of all traffic. Furthermore, with a device CAGR of 7%, it is predicted to have more than 20.6 billion connected devices by 2030. Because of the tremendous expansion of both MDT and users, there is a strong need to broaden the bandwidth to several Terahertz (THz) and increase the average channel capacity to Terabits per second [2]. To that purpose, the wavelength range (0.03–3 mm) or, more accurately, the THz frequency band (0.1–10 THz) began to garner significant attention in the scientific community. Millimeter wave (mmWave) and optical frequency gaps are filled by THz communications, which can enable faster speed data rates compared to mmWave communications. Outdoor THz communication is not affected by the effects of the atmosphere like optical communications are. However, the THz beam may be traced more easily indoors than optical beams, which reduces the mobility of wireless communication devices. Additionally, the reflected pathways in THz communication can be effectively used to improve system performance. THz can also provide UAV services like video surveillance, hotspot seamless coverage, and emergency communications. Nevertheless, despite its appealing properties, THz communication experiences a number of losses, including path-loss, molecular absorption loss, and antenna misalignment loss.

Recently, the performance of UAV-assisted THz wireless communication systems has attracted researchers' attention. In [3], the authors examined the outage performance of reconfigurable intelligent surfaces (RIS)-assisted UAV communications in mixture-gamma multi-path fading with antenna misalignment and UAV disorientation. In the analysis of outages, a THz beam that is orthogonal to the detector plane at the receiver and corresponds to the average position and orientation of the UAV was the sole scenario taken into account. By taking into account a 3D real antenna pattern, the authors of [4] assessed the pointing errors (i.e., the misalignment between the transmit- and receive-antenna) in mmWave and THz communication between unstable transmitter and receiver. They next evaluated the outage performance under α-μ multi-path fading model. The performance of a THz wireless communication system in terms of average channel capacity, average symbol error rate (SER), and outage probability were examined in [5] in random fog conditions and in the presence of pointing error impairments. A scheme that jointly considered power allocation and trajectory optimization to minimize the outage probability of a THz wireless communication system linking a mobile device and a base station (BS) was proposed in [6]. A rate-maximizing strategy that took into account a UAV as a decode-and-forward relay in the full-duplex mode was also put out to increase the BS's coverage area. The authors of [7] reduced the THz transmission delay between the UAV and the ground users while still ensuring that each user's bandwidth and transmit power requirements were met. The authors in [8] considered a wireless communication system in which UAVs and RIS are employed to support THz communications. Moreover, the authors studied the

Manuscript received 21 February 2023; revised 7 May 2023; accepted 15 June 2023. Date of publication 19 June 2023; date of current version 14 November 2023. The review of this article was coordinated by Dr. Cunhua Pan. *(Corresponding author: Osamah S. Badarneh.)*

Osamah S. Badarneh is with the Department of Electrical Engineering, School of Electrical Engineering and Information Technology, German Jordanian University, Amman 11180, Jordan (e-mail: Osamah.Badarneh@gju.edu.jo).

Faissal El Bouanani is with ENSIAS, Mohammed V University in Rabat, Rabat 10000, Morocco (e-mail: f.elbouanani@um5s.net.ma).

Fares Almehmadi is with Electrical Engineering Department, University of Tabuk, Tabuk 71491, Saudi Arabia (e-mail: fal_mehmadi@ut.edu.sa).

Digital Object Identifier 10.1109/TVT.2023.3287288

TABLE I
MATHEMATICAL NOTATIONS AND FUNCTION DEFINITIONS

Notation	Explanation
G_t	Transmit-antenna gain
G_r	Receive-antenna gain
c	Speed of light
f	Operating frequency
d	Transmitter-receiver distance
a	Detector radius
w_0	Beam-waist radius
C_n^2	Refractive-index structure parameter
k_n	Wave-number
$w(d)$	Beam-width
$\rho(d)$	Coherence length
$\mathrm{I}_{p,q}^{m,n}[\cdot]$	I-function [11, Eq. (3.1)]
$\Gamma(\cdot)$	Gamma function [12, Eq. (8.310.1)]
$I_0(\cdot)$	Modified Bessel function of the first kind with zero-order [12, Eq. (8.406.1)]
$\mathrm{erf}(\cdot)$	Error function [12, Eq. (8.250.1)]
$\mathrm{G}_{p,q}^{m,n}[\cdot]$	Meijer's G-function [12, Eq. (9.301)]
$\ln(\cdot)$	Logarithmic function
$\psi(\cdot)$	Digamma function [12, Eq. (8.36)]

problem of maximizing the minimum average achievable rate for all users while taking into consideration the transmit power, the UAV's trajectory, the allocation of THz sub-bands, and the RIS phase shift. In [9], the coverage probability of the network and the area spectral efficiency of the UAV in THz networks were investigated.

Geometric loss arises due to the phenomenon that the receiver can only capture a fraction of power that falls onto the area of its detector, whereas pointing error is due to building sway. It is important to note that pointing errors exacerbate the geometric loss, and therefore THz communication performance is constrained by both losses. However, the model for the generalized geometric loss put forth in [10] and used in this paper takes into account the combined effect of the two types of losses already stated. Our research takes into account the UAV's position and orientation variations as well as the THz beam's non-orthogonality with regard to the receiver's detector plane. The literature has not yet developed this sort of analysis. In this paper, we explicitly provide a generic methodology to analyze the performance of THz communication system operating in generalized fading channels and take into account the effect of the generalized geometric loss.

Motivated by the above, our main contributions can be summarized as follows:

- General and novel analytical expressions for the probability density function (PDF) and the cumulative distribution function (CDF) of the instantaneous SNR under generalized fading channels in the presence of generalized geometric loss are derived.
- General and unique analytical formulas for the outage probability, average SER, and channel capacity are derived based on the derived PDF and CDF expressions.
- Tight approximations of the outage probability, average SER, and channel capacity expressions are provided in the high SNR regime. A very accurate approximate expression for the channel capacity is also found in the low SNR regime.
- As an example, the system performance subject to α-μ THz fading model is analyzed.

The structure of this article is organized as follows. In Section II, we describe the UAV-THz communication systems model as well as the fading channel model. In Section III, we develop a general framework to analyze the system performance under generalized geometric loss. Asymptotic analysis is presented in Section IV. In Section V, we take the α-μ THz fading channel model as an example and then provide the necessary values and parameters to obtain the formulas for the aforementioned performance metrics. Results and discussion considering the α-μ THz fading channel model are given in Section VI, while concluding remarks are outlined in Section VII.

II. SYSTEM AND CHANNEL MODELS

Consider a THz wireless communication system consists of a hovering UAV transmitter and a receiver located at a given distance. Both the transmitter and the receiver are equipped with highly directive antennas, as shown in Fig. 1. Thus, the received signal can be given by

$$g = \sqrt{P_t}\, h_l h_f h_g\, u + n, \tag{1}$$

where P_t denotes the transmitted power, h_l as the path loss, h_f denotes the fading model, h_g as the geometric loss, u as the transmitted signal, and n as a complex additive Gaussian noise with zero-mean and variance σ_0^2.

Let's consider the generalized fading model, in which the PDF of h_f is given in terms of the I-function as

$$f_{h_f}(y) = K\, y^{\varrho-1}\, \mathrm{I}_{p,q}^{m,n}\left[\lambda\, y^{\beta}\,\middle|\, \begin{matrix}(a_i, A_i, \zeta_i)_{i=1:p}\\ (b_i, B_i, \eta_i)_{i=1:q}\end{matrix}\right],\ y>0, \tag{2}$$

where the parameters K, ϱ, λ, β, $(a_i, A_i, \zeta_i)_{1:p}$, and $(b_i, B_i, \eta_i)_{1:q}$ are chosen such that (2) is non-negative, $\zeta_i, \eta_i \in \mathbb{N}$, and $\int_0^\infty f_{h_f}(y)dy = 1$. In addition, the I-function[1] can be

[1]An efficient MATLAB code for evaluating the I-function can be found at https://github.com/osamahbadarneh/I_Function [5].

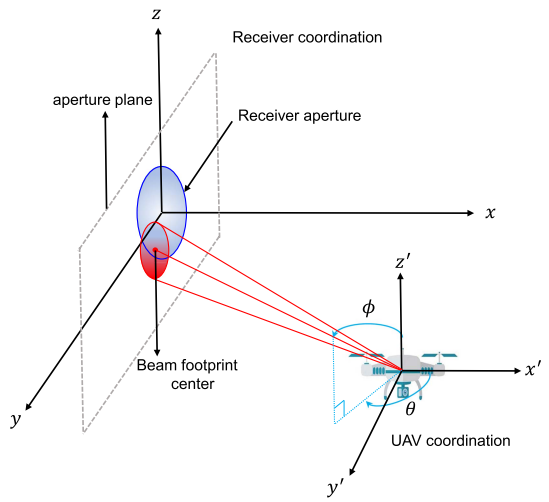

Fig. 1. UAV-based THz communications and system coordinations.

defined in terms of the Mellin-Barnes integral as

$$\mathrm{I}_{p,q}^{m,n}\left[\Theta\left|\begin{matrix}(a_i,A_i,\zeta_i)_{i=1:p}\\(b_i,B_i,\eta_i)_{i=1:q}\end{matrix}\right.\right]=\frac{1}{2\pi j}\int_{\mathfrak{L}}\chi(s)\,\Theta^s ds, \tag{3}$$

where

$$\chi(s)=\frac{\prod_{j=1}^{m}\Gamma^{\eta_j}(b_j-B_j s)\prod_{j=1}^{n}\Gamma^{\zeta_j}(1-a_j+A_j s)}{\prod_{j=m+1}^{q}\Gamma^{\eta_j}(1-b_j+B_j s)\prod_{j=n+1}^{p}\Gamma^{\zeta_j}(a_j-A_j s)}, \tag{4}$$

$j=\sqrt{-1}$, and $\mathfrak{L}$ is a suitable contour integral in the complex s-plane. Note that Fox's H-function can be inferred from the I-function for $\zeta_i=\eta_i=1$. Additionally, when $A_i=B_i=1$, Meijer's G-function can be deduced from the Fox's H-function.

The path-loss h_l is deterministic and given by [13]

$$h_l=\frac{c\sqrt{G_t G_r}}{4\pi f d}\exp\left(-\frac{1}{2}\kappa_\alpha(f)\,d\right), \tag{5}$$

whereby $\kappa_\alpha(f)=y_1(f,\varsigma)+y_2(f,\varsigma)+g(f)$ represents the absorption coefficient [14], in which $y_1(f,\varsigma)=\frac{A(\varsigma)}{B(\varsigma)+(\frac{f}{100c}-c_1)^2}$, $y_2(f,\varsigma)=\frac{C(\varsigma)}{D(\varsigma)+(\frac{f}{100c}-c_2)^2}$, and $g(f)=p_1 f^3+p_2 f^2+p_3 f+p_4$, with $c_1=10.835\,\mathrm{cm}^{-1}$, $c_2=12.664\,\mathrm{cm}^{-1}$, $p_1=5.54\times10^{-37}\,\mathrm{Hz}^{-3}$, $p_2=-3.94\times10^{-25}\,\mathrm{Hz}^{-2}$, $p_3=9.06\times10^{-14}\,\mathrm{Hz}^{-1}$, $p_4=-6.36\times10^{-3}$, while $A(\varsigma)=0.2205\varsigma(0.1303\varsigma+0.0294)$, $B(\varsigma)=(0.4093\varsigma+0.0925)^2$, $C(\varsigma)=2.014\varsigma(0.1702\varsigma+0.0303)$, and $D(\varsigma)=(0.537\varsigma+0.0956)^2$, whereby $\varsigma=\frac{\vartheta}{100}\frac{p_w(T,p)}{p}$, where ϑ, T, and p are respectively refer to the relative humidity, the temperature (in ^{o}K), and the atmospheric pressure. Moreover, the saturated water vapor partial pressure, $p_w(T,p)=6.1121(1.0007+3.46\times10^{-6}p)\exp(\frac{17.502(T-273.15)}{T-32.18})$.

Further, the PDF of the geometric loss h_g arising from the random orientation and fluctuations of the UAV's position is given by [10]

$$f_{h_g}(x)=\frac{\varpi}{A_0}\left(\frac{x}{A_0}\right)^{\frac{(1+q^2)\varpi}{2q}-1} I_0\left(-\frac{(1-q^2)\varpi}{2q}\ln\left(\frac{x}{A_0}\right)\right) \quad 0\le x\le A_0, \tag{6}$$

where $A_0=\mathrm{erf}(\nu_\tau)\,\mathrm{erf}(\nu_\tau)$, $\nu_\tau=\frac{a}{w(d)}\sqrt{\frac{\pi}{2\rho_\tau}}$, $\tau\in\{\min,\max\}$, $w(d)=w_0\sqrt{1+(1+\frac{2w_0^2}{\rho^2(d)})(\frac{c\,d}{\pi f w_0^2})^2}$, $\rho(d)=(0.55C_n^2k_n^2d)^2$, and $k_n=\frac{2\pi f}{c}$. $\rho_{\min}=\frac{2}{\rho_y+\rho_z+\sqrt{(\rho_y-\rho_z)^2+4\rho_{zy}^2}}$, $\rho_{\max}=\frac{2}{\rho_y+\rho_z-\sqrt{(\rho_y-\rho_z)^2+4\rho_{zy}^2}}$, with $\rho_y=\cos^2(\phi)+\sin^2(\phi)\cos^2(\theta)$, $\rho_z=\sin^2(\phi)$, and $\rho_{zy}=-\cos(\phi)\sin(\phi)\sin(\theta)$, $\phi\in[0,\pi]$ denotes the angle between the beam vector and z' axis, whereas $\theta\in[0,2\pi]$ represents the angle between x' axis and the projection of beam vector onto the $x'-y'$ plane, as shown in Fig. 1. In (6), $\varpi=\frac{(1+q^2)k_{\mathrm{mean}}w^2(L)}{4q\Omega}$ is a constant, $k_{\mathrm{mean}}=\frac{k_{\min}+k_{\max}}{2}$ with $k_\tau=\frac{\sqrt{\pi}\rho_\tau\,\mathrm{erf}(\nu_\tau)}{2\nu_\tau\exp(-\nu_\tau^2)}$, $q=\sqrt{\frac{\min\{\lambda_1,\lambda_2\}}{\max\{\lambda_1,\lambda_2\}}}$, and $\Omega=\lambda_1+\lambda_2$, where λ_1 and λ_2 are the eigenvalues of the matrix $\mathbf{\Sigma}$ given by

$$\mathbf{\Sigma}=\begin{bmatrix}\sigma_y^2+\varepsilon_1^2\sigma_x^2+\varepsilon_2^2\sigma_\theta^2 & \varepsilon_1\varepsilon_5\sigma_x^2+\varepsilon_2\varepsilon_4\sigma_\theta^2\\ \varepsilon_1\varepsilon_5\sigma_x^2+\varepsilon_2\varepsilon_4\sigma_\theta^2 & \sigma_z^2+\varepsilon_3^2\sigma_\phi^2+\varepsilon_4^2\sigma_\theta^2+\varepsilon_5^2\sigma_x^2\end{bmatrix}, \tag{7}$$

where $\varepsilon_1=-\tan(\mu_\theta)$, $\varepsilon_2=\frac{-\mu_x}{\cos^2(\mu_\theta)}$, $\varepsilon_3=\frac{-\mu_x}{\sin^2(\mu_\phi)\cos(\mu_\theta)}$, $\varepsilon_4=\frac{-\mu_x\cot(\mu_\phi)\tan(\mu_\theta)}{\cos(\mu_\theta)}$, and $\varepsilon_5=\frac{-\cot(\mu_\phi)}{\cos(\mu_\theta)}$. (μ_θ,μ_ϕ), $(\sigma_\theta,\sigma_\phi)$ represent respectively the means and the standard deviations of the orientation of the UAV, where μ_θ and μ_ϕ respectively given by

$$\mu_\theta=\begin{cases}\tan^{-1}\left(\frac{\mu_y}{\mu_x}\right) & \mu_x>0\\ \pi+\tan^{-1}\left(\frac{\mu_y}{\mu_x}\right), & \text{otherwise}\end{cases} \tag{8}$$

$$\mu_\phi=\pi-\cos^{-1}\left(\frac{\mu_z}{\sqrt{\mu_x^2+\mu_y^2+\mu_z^2}}\right), \tag{9}$$

where (μ_x,μ_y,μ_z) and $(\sigma_x,\sigma_y,\sigma_z)$ denote the means and the standard deviations of the UAV's position. It is worth noting that the smaller the values of $(\sigma_x,\sigma_y,\sigma_z)$ and $(\sigma_\theta,\sigma_\phi)$ are, the more stable the UAV is. Therefore, they are considered as a measure to quantify the quality of the communication link.

Lemma 1: The envelope PDF and CDF of $H=h_l h_f h_g$ can be respectively derived as in (10) and (11), shown at the bottom of this page, where

$$f_H(x)=\frac{K\delta_1}{h_l^{\varrho}A_0^{\varrho-\delta_2}}x^{\varrho-1}\sum_{\ell=0}^{v}(2\ell)!\,\hat{b}_{\ell,v}\left(\frac{\delta_3}{2}\right)^{2\ell}\mathrm{I}_{p+1,q+1}^{m+1,n}\left[\lambda\left(\frac{x}{h_l A_0}\right)^{\beta}\left|\begin{matrix}(a_i,A_i,\zeta_i)_{1:p},(1+\delta_2-\varrho,\beta,2\ell+1)\\(b_i,B_i,\eta_i)_{1:q},(\delta_2-\varrho,\beta,2\ell+1)\end{matrix}\right.\right] \tag{10}$$

$$F_H(x)=\frac{K\delta_1}{h_l^{\varrho}A_0^{\varrho-\delta_2}}x^{\varrho}\sum_{\ell=0}^{v}(2\ell)!\,\hat{b}_{\ell,v}\left(\frac{\delta_3}{2}\right)^{2\ell}\mathrm{I}_{p+2,q+2}^{m+1,n+1}\left[\lambda\left(\frac{x}{h_l A_0}\right)^{\beta}\left|\begin{matrix}(a_i,A_i,\zeta_i)_{1:p},(1-\varrho,\beta,1),(1+\delta_2-\varrho,\beta,2\ell+1)\\(b_i,B_i,\eta_i)_{1:q},(\delta_2-\varrho,\beta,2\ell+1),(-\varrho,\beta,1)\end{matrix}\right.\right] \tag{11}$$

$\delta_1 = \varpi A_0^{-\delta_2}$, $\delta_2 = \frac{(1+q^2)\varpi}{2q}$, $\delta_3 = \frac{(1-q^2)\varpi}{2q}$, and $\hat{b}_{\ell,\upsilon} = \frac{(-1)^\ell (\upsilon+\ell-1)!\, \upsilon^{1-2\ell}}{(\ell!)^2 (\upsilon-\ell)!}$.

Proof: The proof is provided in the Appendix. ■

III. Performance Analysis

We define the instantaneous received SNR as $\Upsilon = \frac{\overline{\gamma}}{\Omega^2} H^2$, with $\overline{\gamma} = \frac{P_t}{\sigma_0^2}$ denotes the average SNR. Thus, using $f_\Upsilon(\gamma) = \frac{1}{2}\sqrt{\frac{\Omega^2}{\overline{\gamma}\gamma}} f_H(\sqrt{\frac{\Omega^2\gamma}{\overline{\gamma}}})$ and (10), $F_\Upsilon(\gamma) = F_H(\sqrt{\frac{\Omega^2\gamma}{\overline{\gamma}}})$ and (11), the PDF and CDF of Υ can be respectively obtained as in (12) and (13), shown at the bottom of this page. Note that the main channel parameters, i.e., ϱ, β, and Ω, in (12) and (13) may represent, for example, the non-linearity of the propagation medium, number of multi-path, and the mean power of the fading channel.

A. Outage Probability

The outage probability can be evaluated via

$$P_{\text{out}} = \Pr[\gamma \le \gamma_0] = F_\Upsilon(\gamma_0), \tag{14}$$

where γ_0 is the required threshold and $F_\Upsilon(\cdot)$ is given in (13).

B. Average Symbol Error Rate

The average SER for various digital modulation schemes can be found using

$$P_s = \frac{\xi \delta^\zeta}{\Gamma(\zeta)} \int_0^\infty \gamma^{\zeta-1} \exp(-\delta\gamma) F_\Upsilon(\gamma)\, \mathrm{d}\gamma, \tag{15}$$

in which the constants parameters (ξ, δ, ζ) depend on the modulation type [15]. Substituting (13) into (15) and using the definition of the I-function, we obtain (16), shown at the bottom of this page. The inner integral in (16), with respect to (w.r.t.) γ, can be solved using [12, eq. (3.381.4)] as

$$\int_0^\infty \gamma^{\frac{\varrho}{2}+\zeta+\frac{\beta s}{2}-1} e^{-\delta\gamma} \mathrm{d}\gamma = \delta^{-\left(\frac{\varrho}{2}+\zeta+\frac{\beta}{2}s\right)} \Gamma\left(\frac{\varrho}{2}+\zeta+\frac{\beta}{2}s\right). \tag{17}$$

Finally, substituting (17) into (16) and using the definition of the I-function, an accurate analytical expression for the average SER can be obtained as in (18) shown at the bottom of this page.

C. Channel Capacity

The average channel capacity subject to a fading channel is given by [16]

$$C_{\text{erg}} = \frac{1}{\ln(2)} \int_0^\infty \ln(1+\gamma) f_\Upsilon(\gamma) \mathrm{d}\gamma. \quad \text{bps/Hz} \tag{19}$$

Replacing the logarithmic function with the Meijer's G-function [17, eq. (8.4.6.5)], representing the I-function in (12) in terms of the Mellin-Barnes integral in (3), and then substituting the results in (19) yields (20), shown at the bottom of the next page. Using [17, eq. (2.24.2.1)], the inner integral in (20) w.r.t.

$$f_\Upsilon(\gamma) = \frac{K\delta_1}{2h_l^\varrho A_0^{\varrho-\delta_2}} \left(\frac{\Omega^2}{\overline{\gamma}}\right)^{\frac{\varrho}{2}} \gamma^{\frac{\varrho}{2}-1} \sum_{\ell=0}^{\upsilon} (2\ell)!\, \hat{b}_{\ell,\upsilon} \left(\frac{\delta_3}{2}\right)^{2\ell} \mathrm{I}_{p+1,q+1}^{m+1,n} \left[\lambda \left(\frac{\Omega^2}{h_l^2 A_0^2 \overline{\gamma}}\right)^{\frac{\beta}{2}} \gamma^{\frac{\beta}{2}} \,\middle|\, \begin{matrix} (a_i, A_i, \zeta_i)_{1:p}, (1+\delta_2-\varrho, \beta, 2\ell+1) \\ (b_i, B_i, \eta_i)_{1:q}, (\delta_2-\varrho, \beta, 2\ell+1) \end{matrix} \right] \tag{12}$$

$$F_\Upsilon(\gamma) = \frac{K\delta_1}{h_l^\varrho A_0^{\varrho-\delta_2}} \left(\frac{\Omega^2}{\overline{\gamma}}\right)^{\frac{\varrho}{2}} \gamma^{\frac{\varrho}{2}} \sum_{\ell=0}^{\upsilon} (2\ell)!\, \hat{b}_{\ell,\upsilon} \left(\frac{\delta_3}{2}\right)^{2\ell} \times \mathrm{I}_{p+2,q+2}^{m+1,n+1} \left[\lambda \left(\frac{\Omega^2}{h_l^2 A_0^2 \overline{\gamma}}\right)^{\frac{\beta}{2}} \gamma^{\frac{\beta}{2}} \,\middle|\, \begin{matrix} (a_i, A_i, \zeta_i)_{1:p}, (1-\varrho, \beta, 1), (1+\delta_2-\varrho, \beta, 2\ell+1) \\ (b_i, B_i, \eta_i)_{1:q}, (\delta_2-\varrho, \beta, 2\ell+1), (-\varrho, \beta, 1) \end{matrix} \right] \tag{13}$$

$$P_s = \frac{K\delta_1 \xi \delta^\zeta}{h_l^\varrho A_0^{\varrho-\delta_2} \Gamma(\zeta)} \left(\frac{\Omega^2}{\overline{\gamma}}\right)^{\frac{\varrho}{2}} \sum_{\ell=0}^{\upsilon} (2\ell)!\, \hat{b}_{\ell,\upsilon} \left(\frac{\delta_3}{2}\right)^{2\ell} \frac{1}{2\pi j} \int_{\mathfrak{L}} \left(\lambda \left(\frac{\Omega^2}{h_l^2 A_0^2 \overline{\gamma}}\right)^{\frac{\beta}{2}} \right)^s \chi(s) \frac{\Gamma^{2\ell+1}(\delta_2-\varrho-\beta s)}{\Gamma^{2\ell+1}(1+\delta_2-\varrho-\beta s)} \times \int_0^\infty \gamma^{\frac{\varrho}{2}+\zeta+\frac{\beta s}{2}-1} e^{-\delta\gamma}\, \mathrm{d}\gamma\, \mathrm{d}s. \tag{16}$$

$$P_s = \frac{\xi K\delta_1}{h_l^\varrho A_0^{\varrho-\delta_2} \Gamma(\zeta)} \left(\frac{\Omega^2}{\delta\,\overline{\gamma}}\right)^{\frac{\varrho}{2}} \sum_{\ell=0}^{\upsilon} (2\ell)!\, \hat{b}_{\ell,\upsilon} \left(\frac{\delta_3}{2}\right)^{2\ell} \times \mathrm{I}_{p+3,q+2}^{m+1,n+2} \left[\lambda \left(\frac{\Omega^2}{h_l^2 A_0^2 \delta\,\overline{\gamma}}\right)^{\frac{\beta}{2}} \,\middle|\, \begin{matrix} (a_i, A_i, \zeta_i)_{1:p}, (1-\varrho, \beta, 1), \left(1-\frac{\varrho}{2}-\zeta, \frac{\beta}{2}, 1\right), (1+\delta_2-\varrho, \beta, 2\ell+1) \\ (b_i, B_i, \eta_i)_{1:q}, (\delta_2-\varrho, \beta, 2\ell+1), (-\varrho, \beta, 1) \end{matrix} \right] \tag{18}$$

γ can be readily obtained as

$$\int_0^\infty \gamma^{\frac{\varrho}{2}+\frac{\beta s}{2}-1} \mathrm{G}_{2,2}^{1,2}\left[\gamma \middle| \begin{matrix} 1,\,1 \\ 1,\,0 \end{matrix}\right] \mathrm{d}\gamma = \frac{\Gamma\left(1+\frac{\varrho}{2}+\frac{\beta}{2}s\right)\Gamma^2\left(-\frac{\varrho}{2}-\frac{\beta}{2}s\right)}{\Gamma\left(1-\frac{\varrho}{2}-\frac{\beta}{2}s\right)}. \tag{21}$$

Substituting (21) back into (20) and applying the definition of the I-function in (3), an accurate analytical expression for the average channel capacity can be obtained as in (22) shown at bottom of this page.

IV. Asymptotic Analysis

Approximate and accurate asymptotic analysis, in the high SNR regime, is provided here. Thus, the coding gain $\mathcal{G}_c$ and the diversity gain $\mathcal{G}_d$ can be easily obtained. To this end, we derive the asymptotic expansion of (3), at $\Theta = 0$. For simplicity, we consider the case when $m = q$ and $n = p = 0$.

A. Asymptotic Outage Probability

Using (13) alongside [12, eq. (8.331.1)], the outage probability can be re-expressed when $m = q$ and $n = p = 0$ as

$$F_\Upsilon(\gamma_0) = \frac{K\delta_1}{h_l^\varrho A_0^{\varrho-\delta_2}} \left(\frac{\Omega^2}{\overline{\gamma}}\right)^{\frac{\varrho}{2}} \gamma_0^{\frac{\varrho}{2}} \sum_{\ell=0}^{\upsilon} (2\ell)! \hat{b}_{\ell,\upsilon} \left(\frac{\delta_3}{2}\right)^{2\ell} \mathcal{I}_\ell, \tag{23}$$

where

$$\mathcal{I}_\ell = \frac{1}{2\pi j} \int_{\mathfrak{L}_0} \underbrace{\frac{\prod_{i=1}^m \Gamma^{\eta_i}(b_i + B_i s)}{(\delta_2 - \varrho + \beta s)^{2\ell+1}(\varrho - \beta s)}}_{\triangleq \chi_0(s)} \Phi_0^{-s} ds, \tag{24}$$

where $\mathfrak{L}_0$ is a complex contour of integration ensuring the convergence of the above Millen-Barnes integral, and

$$\Phi_0 = \underbrace{\lambda \left(\frac{\Omega^2 \gamma_0}{h_l^2 A_0^2}\right)^{\frac{\beta}{2}}}_{\triangleq \Delta_0} \overline{\gamma}^{-\frac{\beta}{2}}, \tag{25}$$

Note that in the high SNR regime, $\Phi \to 0$. To this end, $\mathcal{I}_\ell$ can be asymptotically approximated by the sum of residues evaluated at the top left poles of the above integrand, namely

- $-(\delta_2 - \varrho)/\beta$ of order $2\ell + 1$.
- $-b_{i^*}/B_{i^*}$ of order η_{i^*}, with

$$i^* = \arg \min_{1 \le i \le m} \frac{b_i}{B_i}. \tag{26}$$

For the sake of simplicity, we suppose that all poles of $\Gamma(b_{i^*} + B_{i^*}s)$ are not equal $-(\delta_2 - \varrho)/\beta$, i.e.,

$$\frac{\delta_2 - \varrho}{\beta} \neq \frac{b_{i^*}}{B_{i^*}} + r, r \in \mathbb{N}. \tag{27}$$

Having the two conditions (27) and [18, eq. (1.2.14)], i.e., $\sum_{i=1}^m \eta_i B_i > 0$ satisfied, $\mathcal{I}_\ell$ can be asymptotically approximated as

$$\mathcal{I}_\ell \sim \mathcal{R}_{0,\ell}^{(1)} + \mathcal{R}_{0,\ell}^{(2)}, \tag{28}$$

where $\mathcal{R}_{0,\ell}^{(1)}$ and $\mathcal{R}_{0,\ell}^{(2)}$ account for the residue of $\chi_0(s)\Phi_0^{-s}$ at $-(\delta_2 - \varrho)/\beta$ and $-b_{i^*}/B_{i^*}$, respectively.

1) Evaluation of $\mathcal{R}_{0,\ell}^{(1)}$: As the order of pole $-(\delta_2 - \varrho)/\beta$ equals $2\ell + 1$, it can be ascertained that

$$\mathcal{R}_{0,\ell}^{(1)} = \frac{1}{(2\ell)!} \lim_{s \to -\frac{\delta_2-\varrho}{\beta}} \frac{\partial^{2\ell}}{\partial s^{2\ell}} \left[\Phi_0^{-s} \chi_0(s) \left(s + \frac{\delta_2 - \varrho}{\beta}\right)^{2\ell+1}\right] = \frac{1}{\beta^{2\ell+1}(2\ell)!} \lim_{s \to -\frac{\delta_2-\varrho}{\beta}} \frac{\partial^{2\ell}}{\partial s^{2\ell}} \left(\Phi_0^{-s} \chi_{0,1}(s)\right), \tag{29}$$

where

$$\chi_{0,1}(s) = \frac{\prod_{i=1}^m \Gamma^{\eta_i}(b_i + B_i s)}{\varrho - \beta s}. \tag{30}$$

$$C_{\mathrm{erg}} = \frac{K\delta_1}{2h_l^\varrho A_0^{\varrho-\delta_2} \ln(2)} \left(\frac{\Omega^2}{\overline{\gamma}}\right)^{\frac{\varrho}{2}} \sum_{\ell=0}^{\upsilon} (2\ell)!\, \hat{b}_{\ell,\upsilon} \left(\frac{\delta_3}{2}\right)^{2\ell} \left(\frac{1}{2\pi j}\right) \int_{\mathfrak{L}} \left(\lambda \left(\frac{\Omega^2}{h_l^2 A_0^2 \overline{\gamma}}\right)^{\frac{\beta}{2}}\right)^s \chi(s) \frac{\Gamma^{2\ell+1}(\delta_2 - \varrho - \beta s)}{\Gamma^{2\ell+1}(1 + \delta_2 - \varrho - \beta s)} \times \int_0^\infty \gamma^{\frac{\varrho}{2}+\frac{\beta s}{2}-1} \mathrm{G}_{2,2}^{1,2}\left[\gamma \middle| \begin{matrix} 1,\,1 \\ 0,\,1 \end{matrix}\right] \mathrm{d}\gamma \mathrm{d}s \tag{20}$$

$$C_{\mathrm{erg}} = \frac{K\delta_1}{2h_l^\varrho A_0^{\varrho-\delta_2} \ln(2)} \left(\frac{\Omega^2}{\overline{\gamma}}\right)^{\frac{\varrho}{2}} \sum_{\ell=0}^{\upsilon} (2\ell)!\, \hat{b}_{\ell,\upsilon} \left(\frac{\delta_3}{2}\right)^{2\ell} \times \mathrm{I}_{p+3,q+2}^{m+2,n+1}\left[\lambda \left(\frac{\Omega^2}{h_l^2 A_0^2 \overline{\gamma}}\right)^{\frac{\beta}{2}} \middle| \begin{matrix} (a_i, A_i, \zeta_i)_{1:p}, \left(-\frac{\varrho}{2}, \frac{\beta}{2}, 1\right), (1 + \delta_2 - \varrho, \beta, 2\ell + 1), \left(1 - \frac{\varrho}{2}, \frac{\beta}{2}, 1\right) \\ (b_i, B_i, \eta_i)_{1:q}, (\delta_2 - \varrho, \beta, 2\ell + 1), \left(-\frac{\varrho}{2}, \frac{\beta}{2}, 2\right) \end{matrix}\right] \tag{22}$$

Now, using the Leibniz rule, one gets

$$\mathcal{R}_{0,\ell}^{(1)} = \frac{\Phi_0^{\frac{\delta_2-\varrho}{\beta}}}{\beta^{2\ell+1}(2\ell)!}\sum_{k=0}^{2\ell}\binom{2\ell}{k}\left[-\ln(\Phi_0)\right]^{2\ell-k}\lim_{s\to\frac{\varrho-\delta_2}{\beta}}\chi_{0,1}^{(k)}(s)$$
$$\overset{(a)}{\sim}\frac{\Phi_0^{\frac{\delta_2-\varrho}{\beta}}}{\beta^{2\ell+1}(2\ell)!}\left[\ln(\Phi_0)\right]^{2\ell}\underbrace{\lim_{s\to\frac{\varrho-\delta_2}{\beta}}\chi_{0,1}(s)}_{=\frac{1}{\delta_2}\prod_{i=1}^{m}\Gamma^{\eta_i}\left(b_i+\frac{B_i}{\beta}(\varrho-\delta_2)\right)}, \quad (31)$$

where Step *(a)* holds by noticing that

$$\Phi_0^{\frac{\delta_2-\varrho}{\beta}}\left[\ln(\Phi_0)\right]^{2\ell} \gg \Phi_0^{\frac{\delta_2-\varrho}{\beta}}\left[\ln(\Phi_0)\right]^{2\ell-k}; 1\le k\le 2\ell, \quad (32)$$

when $\Phi_0 \approx 0$.

2) Evaluation of $\mathcal{R}_{0,\ell}^{(2)}$: Analogously, such a residue can be evaluated as

$$\mathcal{R}_{0,\ell}^{(2)} = \frac{1}{(\eta_{i^*}-1)!}\lim_{s\to-\frac{b_{i^*}}{B_{i^*}}}\frac{\partial^{\eta_{i^*}-1}}{\partial s^{\eta_{i^*}-1}}\left[\Phi_0^{-s}\chi_{0,2}(s)\right], \quad (33)$$

where

$$\chi_{0,2}(s) = \frac{\left(s+\frac{b_{i^*}}{B_{i^*}}\right)^{\eta_{i^*}}\prod_{i=1}^{m}\Gamma^{\eta_i}(b_i+B_is)}{(\delta_2-\varrho+\beta s)^{2\ell+1}(\varrho-\beta s)}. \quad (34)$$

In a similar manner to the approximation made in (31), one can check that

$$\mathcal{R}_{0,\ell}^{(2)} = \frac{\Phi_1^{\frac{b_{i^*}}{B_{i^*}}}}{(\eta_{i^*}-1)!}\sum_{k=0}^{\eta_{i^*}-1}(-1)^k\binom{\eta_{i^*}-1}{k}\left[\ln(\Phi_0)\right]^{\eta_{i^*}-1-k}$$
$$\times\lim_{s\to-\frac{b_{i^*}}{B_{i^*}}}\chi_{0,2}^{(k)}(s)$$
$$\sim\frac{\Phi_0^{\frac{b_{i^*}}{B_{i^*}}}}{(\eta_{i^*}-1)!}\left[\ln(\Phi_0)\right]^{\eta_{i^*}-1}\underbrace{\lim_{s\to-\frac{b_{i^*}}{B_{i^*}}}\chi_{0,2}(s)}_{=\frac{\prod_{i=1,i\neq i^*}^{m}\Gamma^{\eta_i}(b_i+B_is)}{B_{i^*}^{\eta_{i^*}}\left(\delta_2-\varrho-\frac{\beta b_{i^*}}{B_{i^*}}\right)^{2\ell+1}\left(\varrho+\frac{\beta b_{i^*}}{B_{i^*}}\right)}}. \quad (35)$$

Utilizing (31) and (35), $\mathcal{I}_\ell$ can be asymptotically approximated as

$$\mathcal{I}_\ell \sim \begin{cases}\mathcal{R}_{0,\ell}^{(1)};\ \delta_2<\varrho+\frac{\beta b_{i^*}}{B_{i^*}}, \eta_{i^*}\le 2\ell+1\\ \mathcal{R}_{0,\ell}^{(2)};\ \delta_2>\varrho+\frac{\beta b_{i^*}}{B_{i^*}}, \eta_{i^*}\ge 2\ell+1\\ \mathcal{R}_{0,\ell}^{(1)}+\mathcal{R}_{0,\ell}^{(2)};\ \text{otherwise}\end{cases}. \quad (36)$$

Substituting (36) into (40), yields

$$F_\Upsilon(\gamma_0) \sim \begin{cases}F_\Upsilon^{(1)}(\gamma_0);\ \delta_2>\varrho+\frac{\beta b_{i^*}}{2B_{i^*}}, \eta_{i^*}\ge 2\upsilon+1\\ F_\Upsilon^{(2)}(\gamma_0);\ \delta_2<\varrho+\frac{\beta b_{i^*}}{2B_{i^*}}, \eta_{i^*}=1\\ F_\Upsilon^{(1)}(\gamma_0)+F_\Upsilon^{(2)}(\gamma_0);\ \text{otherwise}\end{cases}, \quad (37)$$

where $F_\Upsilon^{(1)}(\cdot)$ and $F_\Upsilon^{(2)}(\cdot)$ are defined by (38) and (39), respectively, shown at the bottom of this page. Based on (37), the diversity gain of the system is $G_d = \min(\frac{\delta_2}{2}, \frac{\varrho}{2}+\frac{\beta b_{i^*}}{2B_{i^*}})$. This means that G_d depends on the channel parameters, ϱ and β, and δ_2 which depends on some parameters of the geometric loss such as the UAV's standard deviations of the position, i.e., $\sigma_x, \sigma_y, \sigma_z$, and the UAV's standard deviations of orientation, i.e., $\sigma_\theta, \sigma_\phi$.

B. Asymptotic Average SER

Similarly, P_s can be rewritten when $m=q$ and $n=p=0$ as

$$P_s = \frac{\xi K\delta_1}{h_l^\varrho A_0^{\varrho-\delta_2}\Gamma(\xi)}\left(\frac{\Omega^2}{\delta\overline{\gamma}}\right)^{\frac{\varrho}{2}}\sum_{\ell=0}^{\upsilon}(2\ell)!\hat{b}_{\ell,\upsilon}\left(\frac{\delta_3}{2}\right)^{2\ell}\mathcal{J}_\ell, \quad (40)$$

where

$$\mathcal{J}_\ell = \frac{1}{2\pi j}\int_{\mathfrak{L}_1}\Gamma\left(\frac{\varrho}{2}+\zeta-\frac{\beta}{2}s\right)\chi_0(s)\Phi_1^{-s}ds, \quad (41)$$

and

$$\Phi_1 = \underbrace{\lambda\left(\frac{\Omega^2}{h_l^2A_0^2\delta}\right)^{\frac{\beta}{2}}}_{\triangleq\Delta_1}\overline{\gamma}^{-\frac{\beta}{2}}. \quad (42)$$

It's worth noticing that the integrand in (41) has the identical left poles as the integrand in (41). Besides, if the condition (27) and the inequality $\sum_{i=1}^{m}\eta_iB_i > \beta/2$ are verified, $\mathcal{J}_\ell$ can be asymptotically approximated as

$$\mathcal{J}_\ell \sim \mathcal{R}_{1,\ell}^{(1)} + \mathcal{R}_{1,\ell}^{(2)}, \quad (43)$$

$$F_\Upsilon^{(1)}(\gamma_0) = \frac{K\delta_1\Delta_0^{\frac{b_{i^*}}{B_{i^*}}}\left(\frac{\beta}{2}\right)^{\eta_{i^*}-1}\left(\Omega^2\gamma_0\right)^{\frac{\varrho}{2}}}{h_l^\varrho A_0^{\varrho-\delta_2}(\eta_{i^*}-1)!}\overline{\gamma}^{-\left(\frac{\beta b_{i^*}}{2B_{i^*}}+\frac{\varrho}{2}\right)}\left[\ln\left(\frac{\Omega^2\gamma_0\lambda^{\frac{2}{\beta}}}{h_l^2A_0^2}\right)-\ln(\overline{\gamma})\right]^{\eta_{i^*}-1}$$
$$\times\frac{\prod_{i=1,i\neq i^*}^{m}\Gamma^{\eta_i}\left(b_i-\frac{b_{i^*}B_i}{B_{i^*}}\right)}{B_{i^*}^{\eta_{i^*}}\left(\varrho+\frac{\beta b_{i^*}}{B_{i^*}}\right)}\sum_{\ell=0}^{\upsilon}\frac{(2\ell)!\hat{b}_{\ell,\upsilon}}{\left(\delta_2-\varrho-\frac{\beta b_{i^*}}{B_{i^*}}\right)^{2\ell+1}}\left(\frac{\delta_3}{2}\right)^{2\ell} \quad (38)$$

$$F_\Upsilon^{(2)}(\gamma_0) = \frac{K\delta_1\Delta_0^{\frac{\delta_2-\varrho}{\beta}}\gamma_0^{\frac{\varrho}{2}}\hat{b}_{\upsilon,\upsilon}\Omega^\varrho}{h_l^\varrho A_0^{\varrho-\delta_2}\delta_2\beta}\left(\frac{\delta_3}{4}\right)^{2\upsilon}\overline{\gamma}^{\frac{-\delta_2}{2}}\left[\ln\left(\frac{\Omega^2\gamma_0\lambda^{\frac{2}{\beta}}}{h_l^2A_0^2}\right)-\ln(\overline{\gamma})\right]^{2\upsilon}\prod_{i=1}^{m}\Gamma^{\eta_i}\left(b_i+\frac{B_i}{\beta}(\varrho-\delta_2)\right) \quad (39)$$

where $\mathcal{R}_{1,\ell}^{(1)}$ and $\mathcal{R}_{1,\ell}^{(2)}$ account for the residue of integrand function in (41) at $-(\delta_2-\varrho)/\beta$ and $-b_{i^*}/B_{i^*}$, respectively.

1) Evaluation of $\mathcal{R}_{1,\ell}^{(1)}$: In a similar manner to $\mathcal{R}_{0,\ell}^{(1)}$, it can be seen that

$$\mathcal{R}_{1,\ell}^{(1)} = \frac{1}{\beta^{2\ell+1}(2\ell)!}\lim_{s\to-\frac{\delta_2-\varrho}{\beta}}\frac{\partial^{2\ell}}{\partial s^{2\ell}}\left(\Phi_1^{-s}\chi_{1,1}(s)\right), \tag{44}$$

where

$$\chi_{1,1}(s) = \Gamma\left(\frac{\varrho}{2}+\zeta-\frac{\beta}{2}s\right)\chi_{0,1}(s). \tag{45}$$

Leveraging (32), yields

$$\mathcal{R}_{1,\ell}^{(1)} \sim \frac{\Phi_1^{\frac{\delta_2-\varrho}{\beta}}}{\beta^{2\ell+1}(2\ell)!\delta_2}\left[\ln(\Phi_1)\right]^{2\ell}\Gamma\left(\zeta+\frac{\delta_2}{2}\right) \times\prod_{i=1}^{m}\Gamma^{\eta_i}\left(b_i+\frac{B_i}{\beta}\left(\varrho-\delta_2\right)\right), \tag{46}$$

2) Evaluation of $\mathcal{R}_{2,\ell}^{(2)}$: Likewise, we have

$$\mathcal{R}_{1,\ell}^{(2)} = \frac{1}{(\eta_{i^*}-1)!}\lim_{s\to-\frac{b_{i^*}}{B_{i^*}}}\frac{\partial^{\eta_{i^*}-1}}{\partial s^{\eta_{i^*}-1}}\left[\Phi_1^{-s}\chi_{1,2}(s)\right], \tag{47}$$

where

$$\chi_{1,2}(s) = \Gamma\left(\frac{\varrho}{2}+\zeta-\frac{\beta}{2}s\right)\chi_{0,2}(s). \tag{48}$$

In accordance with (35) and (46), one gets

$$\mathcal{R}_{1,\ell}^{(2)} \sim \frac{\Phi_1^{\frac{b_{i^*}}{B_{i^*}}}\left[\ln(\Phi_1)\right]^{\eta_{i^*}-1}\Gamma\left(\frac{\varrho}{2}+\zeta+\frac{\beta b_{i^*}}{2B_{i^*}}\right)}{(\eta_{i^*}-1)!B_{i^*}^{\eta_{i^*}}\left(\delta_2-\varrho-\frac{\beta b_{i^*}}{B_{i^*}}\right)^{2\ell+1}} \times\frac{\prod_{i=1,i\neq i^*}^{m}\Gamma^{\eta_i}\left(b_i+B_i s\right)}{\varrho+\frac{\beta b_{i^*}}{B_{i^*}}}. \tag{49}$$

It follows using (46) and (49) that $\mathcal{J}_\ell$ can be asymptotically approximated as

$$\mathcal{J}_\ell \sim \begin{cases}\mathcal{R}_{1,\ell}^{(1)};\ \delta_2<\varrho+\frac{\beta b_{i^*}}{B_{i^*}},\eta_{i^*}\leq 2\ell+1\\ \mathcal{R}_{1,\ell}^{(2)};\ \delta_2>\varrho+\frac{\beta b_{i^*}}{B_{i^*}},\eta_{i^*}\geq 2\ell+1\\ \mathcal{R}_{1,\ell}^{(1)}+\mathcal{R}_{1,\ell}^{(2)};\ \text{otherwise}\end{cases}. \tag{50}$$

Finally, plugging (50) into (40), we get

$$P_s \sim \begin{cases}P_s^{(1)};\ \delta_2>\varrho+\frac{\beta b_{i^*}}{2B_{i^*}},\eta_{i^*}\geq 2\upsilon+1\\ P_s^{(2)};\ \delta_2<\varrho+\frac{\beta b_{i^*}}{2B_{i^*}},\eta_{i^*}=1\\ P_s^{(1)}+P_s^{(2)};\ \text{otherwise}\end{cases}, \tag{51}$$

where $P_s^{(1)}$ and $P_s^{(2)}$ are given by (52) and (53), respectively shown at the bottom of this page. Based on (51), the diversity gain of the system is $G_d=\min(\frac{\delta_2}{2},\frac{\varrho}{2}+\frac{\beta b_{i^*}}{2B_{i^*}})$. Similar to the outage probability, the diversity gain G_d depends on the channel parameters, ϱ and β, and δ_2 which depends on some parameters of the geometric loss such as the UAV's standard deviations of the position, i.e., $\sigma_x,\sigma_y,\sigma_z$, and the standard deviations of orientation, i.e., $\sigma_\theta,\sigma_\phi$.

C. Asymptotic Channel Capacity

In the high SNR regime, the average channel capacity can be approximated by [19]

$$C_{\text{erg}}^{\Uparrow} \approx \log_2(\overline{\gamma})+\log_2(e)\frac{\partial}{\partial t}\left.\frac{\mathbb{E}[\gamma^t]}{\overline{\gamma}^t}\right|_{t=0}, \tag{54}$$

where $\frac{\partial}{\partial n}$ denotes the first derivative and $\mathbb{E}[\gamma^t]$ is the t-th moment of the SNR. With the help of (12), $\mathbb{E}[\gamma^t]$ can be expressed as in (55), shown at the bottom of the next page. When $m=q$ and $n=p=0$, utilizing (54) and (56), shown at the bottom of the next page, the asymptotic average channel capacity can obtained as in (57), shown at the bottom of the next page, For low SNR values, i.e., $\overline{\gamma}<<1$, the average channel capacity can be obtained, by setting $t=1$ in (55), and after performing some algebraic manipulations, as in (58), shown at bottom of the next page.

$$P_s^{(1)} = \frac{\xi K\delta_1\Delta_1^{\frac{b_{i^*}}{B_{i^*}}}\left(\frac{\beta}{2}\right)^{\eta_{i^*}-1}}{h_l^{\varrho}A_0^{\varrho-\delta_2}\Gamma(\xi)(\eta_{i^*}-1)!}\left(\frac{\Omega^2}{\delta}\right)^{\frac{\varrho}{2}}\overline{\gamma}^{-\left(\frac{\beta b_{i^*}}{2B_{i^*}}+\frac{\varrho}{2}\right)}\left[\ln\left(\frac{\Omega^2\lambda^{\frac{2}{\beta}}}{h_l^2A_0^2\delta}\right)-\ln(\overline{\gamma})\right]^{\eta_{i^*}-1}\Gamma\left(\frac{\varrho}{2}+\zeta+\frac{\beta b_{i^*}}{2B_{i^*}}\right) \times\frac{\prod_{i=1,i\neq i^*}^{m}\Gamma^{\eta_i}\left(b_i-\frac{b_{i^*}B_i}{B_{i^*}}\right)}{B_{i^*}^{\eta_{i^*}}\left(\varrho+\frac{\beta b_{i^*}}{B_{i^*}}\right)}\sum_{\ell=0}^{\upsilon}\frac{(2\ell)!\widehat{b}_{\ell,\upsilon}}{\left(\delta_2-\varrho-\frac{\beta b_{i^*}}{B_{i^*}}\right)^{2\ell+1}}\left(\frac{\delta_3}{2}\right)^{2\ell} \tag{52}$$

$$P_s^{(2)} = \frac{\xi K\delta_1\Delta_1^{\frac{\delta_2-\varrho}{\beta}}\widehat{b}_{\upsilon,\upsilon}}{h_l^{\varrho}A_0^{\varrho-\delta_2}\Gamma(\xi)\delta_2\beta}\left(\frac{\Omega^2}{\delta}\right)^{\frac{\varrho}{2}}\left(\frac{\delta_3}{4}\right)^{2\upsilon}\overline{\gamma}^{\frac{-\delta_2}{2}} \left[\ln\left(\frac{\Omega^2\lambda^{\frac{2}{\beta}}}{h_l^2A_0^2\delta}\right)-\ln(\overline{\gamma})\right]^{2\upsilon}\Gamma\left(\zeta+\frac{\delta_2}{2}\right)\prod_{i=1}^{m}\Gamma^{\eta_i}\left(b_i+\frac{B_i}{\beta}\left(\varrho-\delta_2\right)\right) \tag{53}$$

V. Special Cases

In the literature, there are three multi-path fading channel models used to characterize the THz communication channel, namely, the α-μ [20], the FTR [21], the gamma-gamma [22], and the mixture of gamma distributions [23]. These distributions can be represented in terms of the I-function and therefore, the analysis presented here is general and can be easily applied. Furthermore, our analysis also can be used for any wireless communication system whose PDF is written in terms of the I-function. For the sake of brevity, we only analysis here the performance over the α-μ fading distribution. However, the rest of distributions have been verified.

A. The α-μ Fading Distribution

With the aid of [24, eq. (1)] and [25, eq. (2.1)], the envelope PDF of the α-μ fading distribution can be represented in terms of the I-function as

$$f_{h_f}(x) = \frac{\alpha\mu^{\mu}}{\Omega^{\alpha\mu}\Gamma(\mu)} x^{\alpha\mu-1}\, \mathrm{I}^{1,0}_{0,1}\left[\frac{\mu}{\Omega^{\alpha}}\, x^{\alpha}\,\middle|\, \begin{matrix} - \\ (0,1,1) \end{matrix}\right], \quad (59)$$

where $\alpha > 0$ is the nonlinearity of the propagation medium, μ is the number of multi-path, and Ω denotes the α-root mean value.

Under the α-μ fading model, the outage probability, the average SER, and the average channel capacity alongside their asymptotic ones can be respectively obtained using (13), (37), (18), (51), (22) and (57) by setting $K = \frac{\alpha\mu^{\mu}}{\Omega^{\alpha\mu}\Gamma(\mu)}$, $\varrho = \alpha\mu$, $\beta = \alpha$, $m = q = 1$ and $n = p = 0$, $i = i^* = 1$, $b_1 = b_{1^*} = 0$, $B_1 = B_{1^*} = 1$, and $\eta_1 = \eta_{1^*} = 1$.

VI. Results and Discussion

Here, we provide some numerical results supported by Monte-Carlo simulation results to investigate the impact of system and channel parameters. Unless stated otherwise, we set $d = 30$ m, $f = 0.3$ THz, $\gamma_0 = 0$ dB, $C_n^2 = 2.3 \times 10^{-9}\ \mathrm{m}^{-2/3}$, $G_t = G_r = 50$ dBi, $\theta = \frac{7\pi}{4}$, and $\phi = \frac{2\pi}{3}$. For the molecular absorption loss in THz band, i.e., $275 - 400$ GHz, $\vartheta = 0.5, T = 296.15^{o}$K, and $p = 101325$ Pa [14]. Note that all series converge rapidly and steadily, requiring only a few terms, i.e., up to 30 terms, to achieve an error less than 10^{-6}. In the figures below, Monte-Carlo simulation results are represented by circle markers. It can be noticed that the Monte-Carlo simulation results are in good agreement with the theoretical results, which verifies the correctness of the analysis.

In Figs. 2, 3, and 4, the performance of the outage probability is plotted for different system and channel parameters. Specifically, in Fig. 2, the impact of the standard deviations of the orientation variables, i.e., σ_θ and σ_ϕ, is investigated. It can be seen that the outage probability performance increases as the standard deviations increase. This is because the larger the values of σ_θ and σ_ϕ are, the more instable the UAV is. In Fig. 3, the impact of the standard deviations of the position

$$\mathbb{E}[\gamma^t] = \frac{K\delta_1}{\beta h_l^{\varrho} A_0^{\varrho-\delta_2}} \left(\frac{\Omega^2}{\overline{\gamma}}\right)^{\frac{\varrho}{2}} \left(\lambda\left(\frac{\Omega^2}{h_l^2 A_0^2 \overline{\gamma}}\right)^{\frac{\beta}{2}}\right)^{-\left(\frac{\varrho}{\beta}+\frac{2t}{\beta}\right)} \sum_{\ell=0}^{v} (2\ell)!\, \hat{b}_{\ell,v} \left(\frac{\delta_3}{2}\right)^{2\ell}$$
$$\times \frac{\Gamma^{2\ell+1}\left(\delta_2 - \varrho + \beta\left(\frac{\varrho}{\beta}+\frac{2t}{\beta}\right)\right) \prod_{i=1}^{m} \Gamma^{\eta_i}\left(b_i + B_i\left(\frac{\varrho}{\beta}+\frac{2t}{\beta}\right)\right) \prod_{i=1}^{n} \Gamma^{\zeta_i}\left(1 - a_i - A_i\left(\frac{\varrho}{\beta}+\frac{2t}{\beta}\right)\right)}{\Gamma^{2\ell+1}\left(1 + \delta_2 - \varrho + \beta\left(\frac{\varrho}{\beta}+\frac{2t}{\beta}\right)\right) \prod_{i=n+1}^{p} \Gamma^{\zeta_i}\left(a_i + A_i\left(\frac{\varrho}{\beta}+\frac{2t}{\beta}\right)\right) \prod_{i=m+1}^{q} \Gamma^{\eta_i}\left(1 - b_i - B_i\left(\frac{\varrho}{\beta}+\frac{2t}{\beta}\right)\right)} \quad (55)$$

$$\frac{\partial}{\partial t}\left.\frac{\mathbb{E}[\gamma^t]}{\overline{\gamma}^t}\right|_{t=0} = \frac{2K\delta_1}{\delta_2\beta^2 h_l^{\varrho} A_0^{\varrho-\delta_2}} \left(\lambda\left(\frac{1}{h_l^2 A_0^2}\right)^{\frac{\beta}{2}}\right)^{\frac{-\varrho}{\beta}} \Gamma\left(\frac{\varrho}{\beta}\right) \sum_{\ell=0}^{v} (2\ell)!\, \hat{b}_{\ell,v} \left(\frac{\delta_3}{2\delta_2}\right)^{2\ell}$$
$$\times \left[-\ln\left(\lambda\left(\frac{\Omega^2}{h_l^2 A_0^2}\right)^{\frac{\beta}{2}}\right) + \psi\left(\frac{\varrho}{\beta}\right) - (2\ell+1)\beta\psi(\delta_2+1) + (2\ell+1)\beta\psi(\delta_2)\right] \quad (56)$$

$$C_{\mathrm{erg}}^{\Uparrow} \approx \log_2(\overline{\gamma}) + \frac{2\log_2(e)K\delta_1}{\delta_2\beta^2 h_l^{\varrho} A_0^{\varrho-\delta_2}} \left(\lambda\left(\frac{1}{h_l^2 A_0^2}\right)^{\frac{\beta}{2}}\right)^{\frac{-\varrho}{\beta}} \Gamma\left(\frac{\varrho}{\beta}\right) \sum_{\ell=0}^{v} (2\ell)!\, \hat{b}_{\ell,v} \left(\frac{\delta_3}{2\delta_2}\right)^{2\ell}$$
$$\times \left[-\ln\left(\lambda\left(\frac{\Omega^2}{h_l^2 A_0^2}\right)^{\frac{\beta}{2}}\right) + \psi\left(\frac{\varrho}{\beta}\right) - (2\ell+1)\beta\psi(\delta_2+1) + (2\ell+1)\beta\psi(\delta_2)\right] \quad (57)$$

$$C_{\mathrm{erg}}^{\Downarrow} \approx \frac{K\delta_1\overline{\gamma}\log_2(e)}{\beta h_l^{\varrho} A_0^{\varrho-\delta_2}(\delta_2+2)\Omega^2} \left(\lambda\left(\frac{1}{h_l^2 A_0^2}\right)^{\frac{\beta}{2}}\right)^{-\left(\frac{\varrho}{\beta}+\frac{2}{\beta}\right)} \Gamma\left(\frac{\varrho}{\beta}+\frac{2}{\beta}\right) \sum_{\ell=0}^{v} (2\ell)!\, \hat{b}_{\ell,v} \left(\frac{\delta_3}{2(\delta_2+2)}\right)^{2\ell} \quad (58)$$

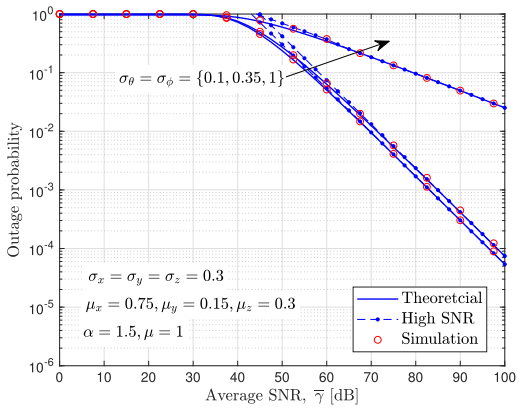

Fig. 2. Outage probability for different values of σ_θ and σ_ϕ.

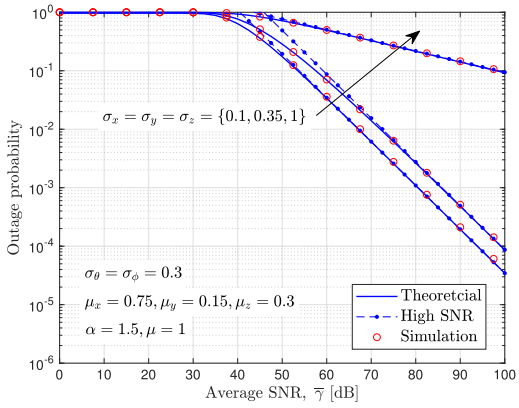

Fig. 3. Outage probability for different values of σ_x, σ_y, and σ_z.

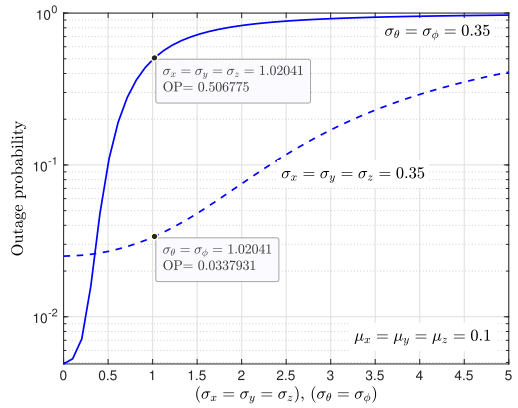

Fig. 4. Outage probability versus $(\sigma_x = \sigma_y = \sigma_z)$ and $(\sigma_\theta = \sigma_\phi)$ for $\alpha = 1.5$, $\mu = 1$, and $\overline{\gamma} = 70$ dB.

variables, i.e., σ_x, σ_y, and σ_z, is studied. The results show that the outage performance improves as σ_x, σ_y, and σ_z decreases. This is because the smaller the values of σ_x, σ_y, and σ_z are, the more stable the UAV is. In Figs. 2 and 3, the asymptotic curves stick to the analytical curves at high SNR values. Note that the slope of the asymptotic curves represents the diversity gain G_d of the outage probability. Hence for the α-μ channel model, $G_d = \min(\frac{\delta_2}{2}, \frac{\alpha\mu}{2})$ since $b_1 = 0$, where δ_2 is given in

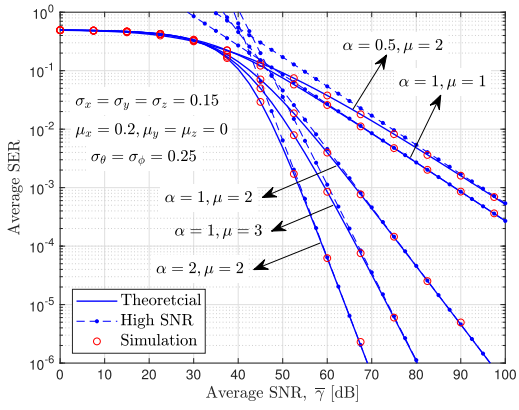

Fig. 5. Average SER for BPSK modulation and different values of α and μ.

Lemma. Thus, in Fig. 2, when $\sigma_\theta = \sigma_\phi = \{0.1, 0.35, 1\}$ the diversity gain, respectively, is $G_d = \{0.75, 0.75, 0.27\}$. The asymptotic curves verify the result in (37) as follows. When $\sigma_\theta = \sigma_\phi = \{0.1, 0.35\}$, the slope of the curves is fixed (i.e., $G_d = 0.75$), while the slope decreases when $\sigma_\theta = \sigma_\phi = 1$ (i.e., G_d decreases from 0.75 to 0.27). Similarly, for Fig. 3, the slope of the curves is fixed when $\sigma_x = \sigma_y = \sigma_z = \{0.1, 0.35\}$ with $G_d = 0.75$ and the slope decreases when $\sigma_x = \sigma_y = \sigma_z = 1$ (i.e., G_d decreases from 0.75 to 0.1821).

Fig. 4 depicts the outage performance as a function of UAV's position when $(\sigma_x = \sigma_y = \sigma_z)$ represented by the solid line and the outage performance as a function of UAV's orientation when $(\sigma_\theta = \sigma_\phi)$ represented by the dashed line. It is clear that the impact of the standard deviations of the position is more pronounced of than that of the standard deviations of the orientation. For example, when $\sigma_\theta = \sigma_\phi = 0.35$ (solid line) the outage probability is about 0.51 at $\sigma_x = \sigma_y = \sigma_z = 1.02$. On the other hand, the outage probability is approximately 0.034 when $\sigma_x = \sigma_y = \sigma_z = 0.35$ (dashed-line) at $\sigma_\theta = \sigma_\phi = 1.02$. This means that the outage probability in the latter case is approximately 93% less than in the former one.

The average SER performance for BPSK modulation under different values of α and μ is shown in Fig. 5. The results demonstrate that the average SER improves as the value of α and(or) μ increase(s). The results also show that the diversity gain depends on the product of α and μ as $G_d = \min(\frac{\delta_2}{2}, \frac{\alpha\mu}{2})$. Therefore, in this figure, the diversity gain G_d is calculated as $G_d = \{2, 1.5, 1, 0.5, 0.5\}$ for $(\alpha, \mu) = \{(2,2), (1,3), (1,2), (1,1), (0.5,2)\}$, respectively. Furthermore, it is clear from the figure that the slope (i.e., diversity gain) of the asymptotic curves increases as the product of α and μ increases, which verifies the asymptotic results in (51).

Fig. 6 shows the influence of the orthogonality and non-orthogonality of the THz beam with respect to (w.r.t.) the plane of the detector. Note that the orthogonal case is obtained when $\theta = 0$ and $\phi = \frac{\pi}{2}$, which corresponds to $\rho_{\max} = \rho_{\min} = 1$ and $\rho_{yz} = 0$. It is clear from the results that the orthogonal case outperforms its counterpart the non-orthogonal case. This means

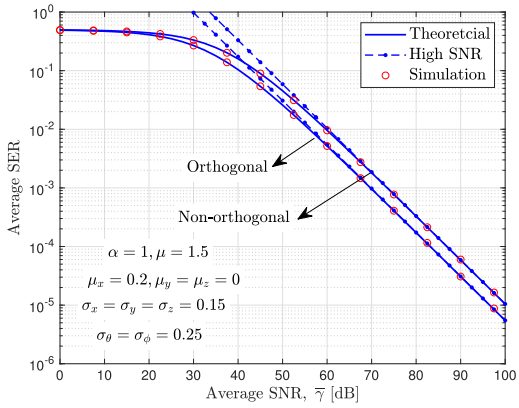

Fig. 6. Average SER for BPSK modulation under orthogonal ($\theta = 0, \phi = \frac{\pi}{2}$) and non-orthogonal ($\theta = \frac{7\pi}{4}, \phi = \frac{2\pi}{3}$) THz beam w.r.t. the detector's plane.

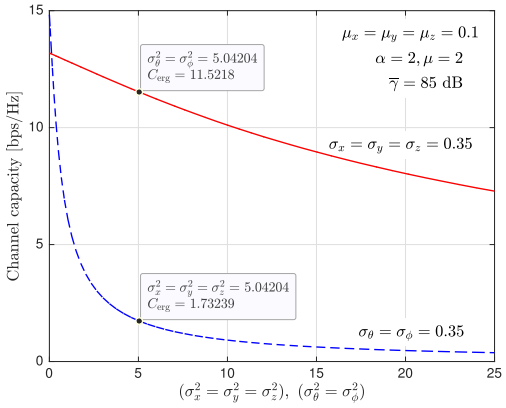

Fig. 7. Average channel capacity for different values of σ_x, σ_y, σ_z, σ_θ, and σ_ϕ. $\mu_x = \mu_y = \mu_z = 0.1$, $\alpha = 2$, $\mu = 2$, and $\overline{\gamma} = 85$ dB.

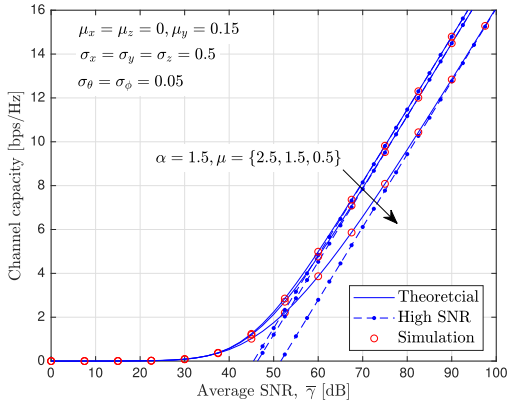

Fig. 8. Channel capacity for different values of μ in the high SNR regime.

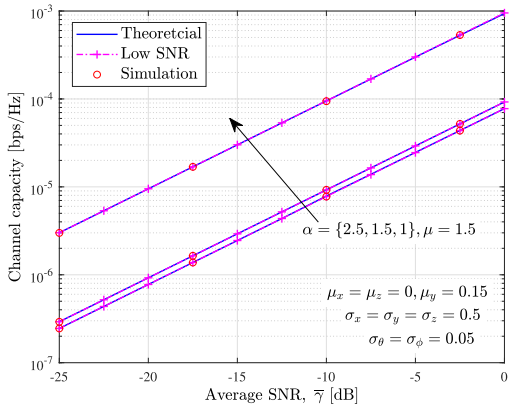

Fig. 9. Channel capacity for different values of α in the low SNR regime.

that the received collected power when the THz beam is orthogonal w.r.t. to the plane of the detector is greater than the non-orthogonal case, which improves the performance. Moreover, the results show that the diversity gain G_d is constant since $\frac{\delta_2}{2} = \frac{\alpha\mu}{2} = 0.75$; thus $G_d = 0.75$. This means that neither the orthogonality nor the non-orthogonality, i.e., the orientation of the UAV, has impact on G_d.

The results in Fig. 7 show that the capacity is much more sensitive to the variances of the position (i.e., σ_x^2, σ_y^2, and σ_z^2), than to the variances of the orientation (i.e., σ_θ^2 and σ_ϕ^2). For instance, when $\sigma_x = \sigma_y = \sigma_z = 0.35$ (solid line), the channel capacity when $\sigma_\theta^2 = \sigma_\phi^2 = 5.04$ is approximately 11.52 [bps/Hz]. Whereas, when $\sigma_\theta = \sigma_\phi = 0.35$ (dashed line), the channel capacity when $\sigma_x^2 = \sigma_y^2 = \sigma_z^2 = 5.04$ is approximately 1.73 [bps/Hz]. In other words, the channel capacity in the latter case is approximately 85% less than the former case. However, the lower the values of σ_x^2, σ_y^2, σ_z^2, σ_θ^2, and σ_ϕ^2 are, the better the performance is.

In Figs. 8 and 9, the channel capacity for different values of α and μ in the high- and low-SNR regimes is respectively plotted. The results show that as μ increases, the channel capacity improves. However, with advancing μ its effect diminished and becomes insignificant. The results in both figures verify the correctness of theoretical results and show the tight match of the asymptotic curves in both regimes.

VII. Conclusion

A framework for analyzing the performance of UAV-aided THz communications over generalized fading channels in the presence of generalized geometric loss is developed. In particular, the PDF and CDF for the received SNR were derived and employed to obtain the exact analytical expressions for the outage probability, average SER, and average channel capacity. Furthermore, tight approximations in the high SNR were provided. These approximations enable us to identify the diversity gain, which depends on the channel parameters such as α and μ, the means and variances of the UAV's position and orientation, and the system parameters such as L, f, a, and w_0. The results demonstrated that the system performance is more sensitive to the variance of UAV's position compared to the variance of the UAV's orientation. As a future work, the analysis in this work can be extended to include intelligent reconfigurable surfaces to assist the UAV communications [26].

$$f_H(x)=\frac{K\delta_1\, x^{\varrho-1}}{h_l^{\varrho}A_0^{\varrho-\delta_2}}\sum_{\ell=0}^{v}\hat{b}_{\ell,v}\left(\frac{\delta_3}{2}\right)^{2\ell}\left(\frac{1}{2\pi j}\right)\int_{\mathfrak{L}}\left(\lambda\left(\frac{x}{h_lA_0}\right)^{\beta}\right)^{s}\chi(s)\int_0^{\infty}t^{2\ell}\,\exp\left(-(\delta_2-\varrho-\beta s)\right)dt\,ds \tag{64}$$

$$f_H(x)=\frac{K\delta_1\, x^{\varrho-1}}{h_l^{\varrho}A_0^{\varrho-\delta_2}}\sum_{\ell=0}^{v}(2\ell)!\,\hat{b}_{\ell,v}\left(\frac{\delta_3}{2}\right)^{2\ell}\left(\frac{1}{2\pi j}\right)\int_{\mathfrak{L}}\left(\lambda\left(\frac{x}{h_lA_0}\right)^{\beta}\right)^{s}\chi(s)\frac{\Gamma^{2\ell+1}(\delta_2-\varrho-\beta s)}{\Gamma^{2\ell+1}(1+\delta_2-\varrho-\beta s)}ds \tag{66}$$

$$F_H(x)=\frac{K\delta_1}{h_l^{\varrho}A_0^{\varrho-\delta_2}}\sum_{\ell=0}^{v}(2\ell)!\,\hat{b}_{\ell,v}\left(\frac{\delta_3}{2}\right)^{2\ell}\left(\frac{1}{2\pi j}\right)\int_{\mathfrak{L}}\left(\lambda\left(\frac{1}{h_lA_0}\right)^{\beta}\right)^{s}\chi(s)\frac{\Gamma^{2\ell+1}(\delta_2-\varrho-\beta s)}{\Gamma^{2\ell+1}(1+\delta_2-\varrho-\beta s)}\int_0^{x}u^{\varrho+\beta s-1}du\,ds \tag{67}$$

$$F_H(x)=\frac{K\delta_1\, x^{\varrho}}{h_l^{\varrho}A_0^{\varrho-\delta_2}}\sum_{\ell=0}^{v}(2\ell)!\,\hat{b}_{\ell,v}\left(\frac{\delta_3}{2}\right)^{2\ell}\left(\frac{1}{2\pi j}\right)\int_{\mathfrak{L}}\left(\lambda\left(\frac{x}{h_lA_0}\right)^{\beta}\right)^{s}\chi(s)\frac{\Gamma^{2\ell+1}(\delta_2-\varrho-\beta s)\,\Gamma(\varrho+\beta s)}{\Gamma(1+\varrho+\beta s)\,\Gamma^{2\ell+1}(1+\delta_2-\varrho-\beta s)}ds \tag{69}$$

APPENDIX
PROOF OF LEMMA 1

The PDF of $H=h_lh_fh_g$ can be obtained via

$$f_H(x)=\frac{1}{h_l}\int_{\frac{x}{h_lA_0}}^{\infty}\frac{1}{y}f_{h_f}(y)f_g\left(\frac{x}{h_ly}\right)dy. \tag{60}$$

Thus, substituting (2) and (6) into (60) yields

$$f_H(x)=\frac{K\delta_1x^{\delta_2-1}}{h_l^{\delta_2}}\int_{\frac{x}{h_lA_0}}^{\infty}y^{\varrho-\delta_2-1}\,\mathrm{I}_{p,q}^{m,n}\left[\lambda\,y^{\beta}\,\middle|\,\begin{matrix}(a_i,A_i,\zeta_i)_{1:p}\\(b_i,B_i,\eta_i)_{1:q}\end{matrix}\right]\times I_0\left(-\delta_3\ln\left(\frac{x}{h_lA_0y}\right)\right)dy. \tag{61}$$

To the best of the authors' knowledge, there is no solution to the integral in (61) in its current form. However, the function $I_0(\cdot)$ can be represented in terms of its polynomial given in [27, eq. (13)][2]. Thus,

$$f_H(x)=\frac{K\delta_1x^{\delta_2-1}}{h_l^{\delta_2}}\sum_{\ell=0}^{v}\hat{b}_{\ell,v}\left(\frac{\delta_3}{2}\right)^{2\ell}\int_{\frac{x}{h_lA_0}}^{\infty}y^{\varrho-\delta_2-1}\times\mathrm{I}_{p,q}^{m,n}\left[\lambda\,y^{\beta}\,\middle|\,\begin{matrix}(a_i,A_i,\zeta_i)_{1:p}\\(b_i,B_i,\eta_i)_{1:q}\end{matrix}\right]\left(-\ln\left(\frac{x}{h_lA_0y}\right)\right)^{2\ell}dy. \tag{62}$$

Now, let $t=-\ln(\frac{x}{h_lA_0y})$. Thus, after some algebraic manipulations, the integral in (62) reduces to

$$f_H(x)=\frac{K\delta_1x^{\varrho-1}}{h_l^{\varrho}A_0^{\varrho-\delta_2}}\sum_{\ell=0}^{v}\hat{b}_{\ell,v}\left(\frac{\delta_3}{2}\right)^{2\ell}\int_0^{\infty}t^{2\ell}\,\exp\left(-(\delta_2-\varrho)t\right)\times\mathrm{I}_{p,q}^{m,n}\left[\lambda\left(\frac{x}{h_lA_0}\exp\left(t\right)\right)^{\beta}\,\middle|\,\begin{matrix}(a_i,A_i,\zeta_i)_{1:p}\\(b_i,B_i,\eta_i)_{1:q}\end{matrix}\right]dt. \tag{63}$$

[2]The convergence and truncation error for the polynomial are discussed in details in [27].

With the help of (3), we obtain (64), shown at the top of this page. In (64), the inner integral w.r.t. t can be solved by respectively using [12, eq. (3.381.4)] and [12, eq. (8.331.1)] as

$$\int_0^{\infty}t^{2\ell}\,\exp\left(-(\delta_2-\varrho-\beta s)t\right)dt=(2\ell)!\,\frac{\Gamma^{2\ell+1}(\delta_2-\varrho-\beta s)}{\Gamma^{2\ell+1}(1+\delta_2-\varrho-\beta s)}. \tag{65}$$

Substituting (65) into (64), yields (66), shown at the top of this page. Finally, applying the definition of the I-function to (66), an accurate analytical expression for the envelope PDF of H is obtained as in (10). The corresponding CDF can be obtained using the PDF in (66). Thus, we obtain (67), shown at the top of this page. Moreover, the inner integral in (67) w.r.t. u can be solved as

$$\int_0^{x}u^{\varrho+\beta s-1}du=x^{\varrho+\beta s}\frac{\Gamma(\varrho+\beta s)}{\Gamma(1+\varrho+\beta s)}. \tag{68}$$

Substituting the result of (68) into (67), yields (69), shown at the top of this page. Finally, using the definition of the I-function in (3), the CDF in (11) is obtained. This completes the proof of Lemma 1.

REFERENCES

[1] "Cisco visual networking index: Global mobile data traffic forecast update, 2017–2022," Feb. 2019. Accessed: Jun. 24, 2023. [Online]. Available: http://media.mediapost.com/uploads/CiscoForecast.pdf

[2] I. F. Akyildiz, J. M. Jornet, and C. Han, "TeraNets: Ultra-broadband communication networks in the terahertz band," *IEEE Wireless Commun.*, vol. 21, no. 4, pp. 130–135, Aug. 2014.

[3] A.-A. A. Boulogeorgos, A. Alexiou, and M. D. Renzo, "Outage performance analysis of RIS-assisted UAV wireless systems under disorientation and misalignment," *IEEE Trans. Veh. Technol.*, vol. 71, no. 10, pp. 10712–10728, Oct. 2022.

[4] M. T. Dabiri and M. Hasna, "Pointing error modeling of mmWave to THz high-directional antenna arrays," *IEEE Wireless Commun. Lett.*, vol. 11, no. 11, pp. 2435–2439, Nov. 2022.

[5] O. S. Badarneh, "Performance analysis of terahertz communications in random fog conditions with misalignment," *IEEE Wireless Commun. Lett.*, vol. 11, no. 5, pp. 962–966, May 2022.

[6] S. Farrag, E. Maher, A. El-Mahdy, and F. Dressler, "Performance analysis of UAV assisted mobile communications in THz channel," *IEEE Access*, vol. 9, pp. 160104–160115, 2021.

[7] L. Xu et al., "Joint location, bandwidth and power optimization for THz-enabled UAV communications," *IEEE Commun. Lett.*, vol. 25, no. 6, pp. 1984–1988, Jun. 2021.
[8] Y. Pan, K. Wang, C. Pan, H. Zhu, and J. Wang, "UAV-assisted and intelligent reflecting surfaces-supported terahertz communications," *IEEE Wireless Commun. Lett.*, vol. 10, no. 6, pp. 1256–1260, Jun. 2021.
[9] X. Wang et al., "Performance analysis of terahertz unmanned aerial vehicular networks," *IEEE Trans. Veh. Technol.*, vol. 69, no. 12, pp. 16330–16335, Dec. 2020.
[10] M. Najafi, H. Ajam, V. Jamali, P. D. Diamantoulakis, G. K. Karagiannidis, and R. Schober, "Statistical modeling of FSO fronthaul channel for drone-based networks," in *Proc. IEEE Int. Conf. Commun.*, 2018, pp. 1–7.
[11] A. K. Rathie, "A new generalization of generalized hypergeometric functions," *Le Matematiche*, vol. 52, no. 2, pp. 297–310, Mar. 1997.
[12] I. S. Gradshteyn and I. M. Ryzhik, *Table of Integrals, Series, and Products*, 7th ed. San Diego, CA, USA: Academic Press, 2007.
[13] W. Tang et al., "Wireless communications with reconfigurable intelligent surface: Path loss modeling and experimental measurement," *IEEE Trans. Wireless Commun.*, vol. 20, no. 1, pp. 421–439, Jan. 2021.
[14] J. Kokkoniemi, J. Lehtomäki, and M. Juntti, "Simplified molecular absorption loss model for 275–400 Gigahertz frequency band," in *Proc. IET 12th Eur. Conf. Antennas Propag.*, 2018, pp. 1–5.
[15] O. S. Badarneh, R. Derbas, F. S. Almehmadi, F. El Bouanani, and S. Muhaidat, "Performance analysis of FSO communications over F turbulence channels with pointing errors," *IEEE Commun. Lett.*, vol. 25, no. 3, pp. 926–930, Mar. 2021.
[16] M. K. Simon and M.-S. Alouini, *Digital Communications Over Fading Channels*, 2nd ed. New York, NY, USA. Wiley, 2005.
[17] A. P. Prudnikov et al., *Integrals, and Series: More Special Functions*, vol. 3. New York, NY, USA: Gordon & Breach Sci. Publ., 1990.
[18] A. Kilbas and M. Saigo, *H-Transforms: Theory and Applications* (Analytical Method and Special Function), 1st ed. Boca Raton, FL, USA: CRC Press, 2004.
[19] F. Yilmaz and M.-S. Alouini, "Novel asymptotic results on the high-order statistics of the channel capacity over generalized fading channels," in *Proc. IEEE 13th Int. Workshop Signal Process. Adv. Wireless Commun.*, 2012, pp. 389–393.
[20] E. N. Papasotiriou et al., "An experimentally validated fading model for THz wireless systems," *Sci. Rep.*, vol. 11, Sep. 2021.
[21] H. Duet al., "Reconfigurable intelligent surface aided terahertz communications under misalignment and hardware impairments," *CoRR*, Dec. 2020. [Online]. Available: https://arxiv.org/abs/2012.00267
[22] J. Ye, S. Dang, G. Ma, O. Amin, B. Shihada, and M.-S. Alouini, "On outage performance of terahertz wireless communication systems," *IEEE Trans. Commun.*, vol. 70, no. 1, pp. 649–663, Jan. 2022.
[23] K. Tekbıyık, A. R. Ekti, G. K. Kurt, A. Gürçin, and S. Yarkan, "Modeling and analysis of short distance sub-terahertz communication channel via mixture of Gamma distribution," *IEEE Trans. Veh. Technol.*, vol. 70, no. 4, pp. 2945–2954, Apr. 2021.
[24] M. D. Yacoub, "The α-μ distribution: A general fading distribution," in *Proc. 13th IEEE Int. Symp. Pers., Indoor Mobile Radio Commun.*, 2002, pp. 629–633.
[25] P. Vellaisamy and K. K. Kataria, "The I-function distribution and its extensions," *Theory Probability Appl.*, vol. 63, no. 2, pp. 227–245, 2018.
[26] X. Pang, M. Sheng, N. Zhao, J. Tang, D. Niyato, and K.-K. Wong, "When UAV meets IRS: Expanding air-ground networks via passive reflection," *IEEE Wireless Commun.*, vol. 28, no. 5, pp. 164–170, Oct. 2021.
[27] L. Li and F. Gross, "A new polynomial approximation for J_v Bessel functions," *J. Comput. Appl. Math.*, vol. 183, pp. 1220–1225, Dec. 2006.